

Preparation and ESR Detection of a Ground-State Nonet Hydrocarbon as a Model for One-Dimensional Organic Ferromagnets

Yoshio Teki,[†] Takeji Takui,[†] Koichi Itoh,^{*†} Hiizu Iwamura,^{*†} and Kazumasa Kobayashi[‡]

Contribution from the Department of Chemistry, Faculty of Science, Osaka City University, Sujimoto, Sumiyoshi-ku, Osaka 558, Japan, and the Institute for Molecular Science, Myodaiji, Okazaki 444, Japan. Received July 12, 1985

Abstract: The spin state and molecular conformation of a novel alternant hydrocarbon, *m*-phenylenebis[(diphenylmethylene-3-yl)methylene] (**1**), have been studied by electron-spin resonance. The tetracarbene **1** was generated by the photolysis of the corresponding tetradiazo compound, *m*-phenylenebis[*m*-(α -diazobenzyl)phenyldiazomethane] (**2**), which was synthesized as follows: The reaction of *m*-tolylmagnesium bromide with isophthalonitrile produced 1,3-di-(*m*-toluoyl)benzene, which was oxidized in two steps to isophthalophenone-3,3'-dicarboxylic acid. The Friedel-Crafts reaction of the bis(acid chloride) in benzene gave 3,3'-dibenzoylisophthalophenone. The corresponding tetrahydrazone was oxidized with active MnO₂ to give **2**. The eight-line ESR spectrum due to **1** was obtained when benzophenone single crystals doped with **2** were irradiated with the 405-nm mercury line at 4.2 K. The relative separation and integrated intensities of the lines are in accord with the $\Delta M_S = \pm 1$ allowed transitions between the fine-structure sublevels of the nonet spin manifold in the high-field limit. The resonance fields and signal intensities observed at the K band (25 GHz) were well-reproduced by a third-order perturbation calculation based on the spin Hamiltonian $\mathcal{H} = g\beta\mathbf{SH} + D[S_z^2 - S(S+1)/3] + E(S_x^2 - S_y^2)$ with $g = 2.002$, $D = +0.03161 \text{ cm}^{-1}$, $E = -0.00394 \text{ cm}^{-1}$, and $S = 4$, proving **1** to be in the nonet state. Only the nonet spectrum was observed after photolysis. The temperature dependence of its total signal intensity in the range 1.8–56 K showed the observed nonet state to be the ground state, while the other triplet, quintet, and septet states also expected from the eight parallel spins are located at least 300 cm⁻¹ above the ground state. When the sample was warmed, the spectrum showed irreversible spectral transitions at 64 K to two sets of new nonet signals and again at 92 K to a fourth set of nonet signals, which finally decayed out at 160 K. The transitions are ascribable to molecular conformation changes, which led to four nonet isomers. A semiempirical calculation of their fine-structure tensors has been carried out assuming the dipole-dipole interaction between the electron spins and the one-center $n-\pi$ interactions on the divalent carbon atoms to be predominant. By fitting them to the observed fine-structure tensors, we obtained the most probable conformations for each of the four nonet isomers. Evidence for a one-photon process in the photodissociation of **2** into **1** was also obtained. The novel hydrocarbon described in this paper has the highest spin multiplicity so far reported among organic as well as inorganic molecules. This unusually high-spin multiplicity results from the topological symmetry. Such a high-spin state is relevant to the design of organic ferromagnets.

Most known organic molecules have singlet ground states and are therefore usually diamagnetic. Paramagnetic organic compounds, less frequently, are usually free radicals. Their doublet ground state stems from an odd number of electrons. These magnetic properties contrast with those of inorganic compounds for which high-spin multiplicity in the ground state is not unusual. Until the early 1960s, this difference was held to reflect the low symmetry of organic molecules: from the group theoretical point of view, at most triply degenerate molecular orbitals could be found. Therefore, Hund's rule predicts a maximum spin of $3/2$. In fact, organic molecules with the maximum spin consistent with their symmetry have not been detected yet. The pentachlorocyclopentadienyl cation¹ and the cyclopentadienyl cation² have such degenerate orbitals. They have been synthesized and they have been proven to have a triplet ground state. Due to their C₅ symmetry, their highest occupied molecular orbitals are doubly degenerate, hence the parallel spins. It should be noted that such degeneracy can be lifted by Jahn-Teller distortion as observed with the pentaphenylcyclopentadienyl cation, a singlet in the ground state.^{3,4} For organic molecules, therefore, high-spin multiplicity may not be expected from the degeneracy due to geometrical symmetry.

Higuchi did the early theoretical work on organic high-spin molecules in 1963. He calculated the fine-structure parameters due to electron spin-spin interactions for several aromatic hydrocarbons being hypothetical at that time.^{5,6} The first high-spin molecule was reported by one of us (K. I.)⁷ and subsequently by Wasserman et al.⁸ in 1967. This aromatic hydrocarbon, *m*-phenylenebis(phenylmethylene), is a quintet in the electronic ground state. Its fine-structure parameters obtained by electron-spin resonance (ESR) were in reasonable agreement with

the values predicted by Higuchi.^{5,9} This hydrocarbon was a prototype for the series of high-spin hydrocarbons detected thereafter: *m*-phenylenebis(methylene) ($S = 2$),⁸ benzene-1,3,5-tris(phenylmethylene) ($S = 3$),¹⁰ biphenyl-3,3'-bis(phenylmethylene) ($S = 0, 1, 2$),¹¹ 1,3,5-benzenetriyltris[bis(biphenyl-4-yl)methyl] ($S = 3/2$),¹² and 3,3'-diphenylmethylenebis(phenylmethylene) ($S = 3$).¹³ In addition, quintet and septet nitrenes isoelectronic with the above-mentioned quintet and septet hydrocarbons have been detected since.^{8,14}

Recently, we published a preliminary report of the detection by single-crystal ESR of an aromatic hydrocarbon, *m*-phenylenebis[(diphenylmethylene-3-yl)methylene] (**1**) with nonet spin multiplicity ($S = 4$) in the electronic ground state.¹⁵ Static

(1) Breslow, R.; Hill, R.; Wasserman, E. *J. Am. Chem. Soc.* **1964**, *86*, 5349-5350.

(2) Saunders, M.; Berger, R.; Jaffe, A.; McBride, J. M.; O'Neill, J.; Breslow, R.; Hoffman, J. M., Jr.; Perchonock, C.; Wasserman, E.; Hutton, R. S.; Kuck, V. J. *J. Am. Chem. Soc.* **1973**, *95*, 3017-3018.

(3) Breslow, R.; Chang, H. W.; Yager, W. A. *J. Am. Chem. Soc.* **1963**, *85*, 2033-2034.

(4) Breslow, R.; Chang, H. W.; Hill, R.; Wasserman, E. *J. Am. Chem. Soc.* **1967**, *89*, 1112-1119.

(5) Higuchi, J. *J. Chem. Phys.* **1963**, *38*, 1237-1245.

(6) Higuchi, J. *J. Chem. Phys.* **1963**, *39*, 1847-1852.

(7) Itoh, K. *Chem. Phys. Lett.* **1967**, *1*, 235-238.

(8) Wasserman, E.; Murray, R. W.; Yager, W. A.; Trozzolo, A. M.; Smolinsky, G. *J. Am. Chem. Soc.* **1967**, *89*, 5076-5078.

(9) Higuchi, J. *Bull. Chem. Soc. Jpn.* **1970**, *43*, 3773-3779.

(10) Takui, T.; Itoh, K. *Chem. Phys. Lett.* **1973**, *19*, 120-124.

(11) Itoh, K. *Pure Appl. Chem.* **1978**, *50*, 1251-1259.

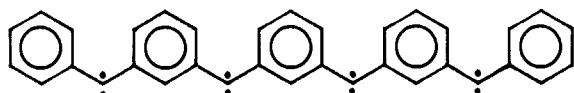
(12) Reibisch, K.; Kothe, H.; Brickmann, J. *Chem. Phys. Lett.* **1972**, *17*, 86-89. Brickmann, J.; Kothe, G. *J. Chem. Phys.* **1973**, *59*, 2807-2814.

(13) Teki, Y.; Takui, T.; Yagi, H.; Itoh, K.; Iwamura, H. *J. Chem. Phys.* **1985**, *83*, 539-547.

(14) Wasserman, E.; Scheller, K.; Yager, W. A. *Chem. Phys. Lett.* **1968**, *2*, 259-260.

[†] Osaka City University.

[‡] Institute for Molecular Science.



(1)

magnetic susceptibility measurements have also confirmed the nonet ground state.¹⁶ This is the highest spin multiplicity known to date for an organic molecule. In inorganic molecules, the nonet spin multiplicity is also the highest. It is found in GdO, recently reported by Weltner et al.,¹⁷ for which the nonet ground state is attributed to the $4f^7 5d\sigma$ electronic configuration.

The unusually high spin multiplicity of the above-mentioned organic molecules arises from a characteristic property of non-bonding molecular orbitals (NBMO) in alternant hydrocarbons (AH). This was pointed out as early as 1950 by Longuet-Higgins.¹⁸ His rule states that an AH has at least $N - 2T$ singly occupied NBMO's where N is the number of carbon atoms in the AH and T is the maximum number of double bonds occurring in any resonance structure. The $(N - 2T)$ -fold degeneracy is thus due to topological symmetry and has been termed "topological degeneracy".¹¹ AH's with such degenerate NBMO's may be further classified into two types, according to whether their NBMO's can be confined to disjoint sets of atoms: for disjoint AH's possible open-shell spin states are nearly degenerate with each other, while for nondisjoint AH's the highest spin state lies well below the other states. This was shown theoretically for diradicals by Borden and Davidson¹⁹ and experimentally for quintet molecules by us.¹¹ Molecule **1** and its homologues belong to the nondisjoint AH. Recently, a valence bond approach to high-spin molecules has been proposed by Ovchinnikov²⁰ and Klein.^{21,22} It predicts the spin multiplicity of AH's on the basis of the Heisenberg Hamiltonian theory of Lieb and Mattis.²³

Molecule **1** is an even AH. It may reasonably be assumed, by analogy with the quintet *m*-phenylenebis(phenylmethylene),^{7,8} that one of the unpaired electrons on each divalent carbon is conjugated with the π system of the benzene rings. The other unpaired electron remains in the nonbonding "n" orbital localized on the divalent carbon atom. Thus, **1** has singly occupied, 4-fold-degenerate NBMO's. In addition, it has four n orbitals, which are nearly degenerate with the NBMO's and which are also singly occupied. The meta substitution in **1** is essential to the topological degeneracy of the NBMO's. Eight spins when placed in eight nearly degenerate molecular orbitals should be parallel according to Hund's second rule, as confirmed by our recent experiments.¹⁵ The parallel spins in the NBMO's are delocalized over the whole molecule, and they are exchange-coupled ferromagnetically to the localized spins in the n orbitals on the divalent carbon atoms. This $n-\pi$ interaction indeed closely resembles the $s-d$ interaction²⁴ between conducting s electrons and localized d electrons in ferromagnetic dilute alloys.

It is important to note that, contrary to the degeneracy due to geometrical symmetry, there exists in principle no limitation to the degree of topological degeneracy: any desired N and/or T can be obtained with properly designed molecules. Therefore, if

we consider a long chain extension of the unit in **1**, pseudo-one-dimensional organic ferromagnets may be expected. Mataga²⁵ and one of us (K. I.)²⁶ have discussed a possible electronic structure for such polymers on the basis of a simple molecular orbital theory. Recently, a more advanced molecular orbital approach has been reported on the band structure and spin densities for such polymers by Tyutyulkov et al.;²⁷ within the Hartree-Fock approximation, correlation between the π electrons leads to the ferromagnetic ground state. On the other hand, using the periodic Kondo-Hubbard model and taking into account the localized n spins, Nasu has calculated the band structure for a one-dimensional polymer, an extension of **1**.²⁸ It is shown that within the mean field theory, the ferromagnetic ground state is always stable as a result of cooperation between the two kinds of correlations and the topological structure. One-dimensional magnetic systems containing transition-metal ions such as CsNiF_3 ,²⁹ $(\text{CH}_3)_4\text{NMnCl}_3$,³⁰ $\text{TMNB}((\text{CH}_3)_4\text{NNiBr}_3)$,³¹ etc., are a topic of considerable interest in physics.³²

On the other hand, with their valence bond approach to organic ferromagnets, Ovchinnikov²⁰ and Klein et al.²¹ have, recently, proposed macromolecules containing heteroatoms such as B, N, O, and S together with AH polymers.

Originally proposed by McConnell,³³ another idea for the molecular design of organic ferromagnets exploits the charge transfer between triplet donors and singlet acceptors (or between singlet donors and triplet acceptors). An attempt to synthesize triplet acceptors such as dications of hexaaminotriphenylene and hexaaminobenzene derivatives was recently made by Breslow et al.^{34,35}

In the present paper, we describe a synthesis of the diazo precursor of **1**, *m*-phenylenebis[*m*-(α -diazobenzyl)phenyldiazomethane] (**2**). We report the ESR investigation of the X-band and K-band spectra of **1** in single crystals of benzophenone after photolysis, which prove that **1** is nonet in the electronic ground state. The observed *g* and fine-structure tensors for the nonet state are referred to the structure of **1**. The molecular conformation in the host crystal is determined from the observed fine-structure tensor with the help of a semiempirical calculation: interesting conformational changes occur in the host crystal. Finally, a remarkable photochemical phenomenon found during photodissociation into **1** suggests a one-photon process in the host crystal.

Experimental Section

A. Materials. ¹H (99.6 MHz) and ¹³C NMR (25.0 MHz) spectra were recorded on a JEOL FX-100 instrument. Some ¹H NMR spectra were also obtained on a JNM GX-400 (400 MHz) spectrometer. IR spectra were obtained in KBr disks unless otherwise stated on a JASCO IRA-1 spectrometer. Melting points are not corrected.

3,3'-Dimethylisophthalophenone. To the ice-cooled Grignard reagent prepared from 40 g (0.234 mol) of *m*-bromotoluene and 7.39 g (0.303 mol) of magnesium in 180 mL of dry ether was added with stirring a suspension of 12.3 g (0.096 mol) of isophthalonitrile in 50 mL of dry benzene. The mixture was allowed to warm to room temperature and stirred for 1 h. Aqueous hydrochloric acid (3 N) was slowly added and stirred for 8 h. The organic layer was washed with water and dried over magnesium sulfate. Colorless needles (24.1 g, 80%) were obtained after recrystallization from petroleum ether: mp 101–102 °C; IR ν_{CO} 1660 cm^{-1} ; ¹H NMR (CDCl_3) δ 2.53 (s, 6 H), 7.30–8.25 (m, 12 H). Anal. Calcd for $\text{C}_{22}\text{H}_{18}\text{O}_2$: C, 84.05; H, 5.77. Found: C, 83.90; H, 5.80.

(15) Teki, Y.; Takui, T.; Itoh, K.; Iwamura, H.; Kobayashi, K. *J. Am. Chem. Soc.* **1983**, *105*, 3722–3723.

(16) Sugawara, T.; Bandow, S.; Kimura, K.; Iwamura, H.; Itoh, K. *J. Am. Chem. Soc.* **1984**, *106*, 6449–6450; **1986**, *108*, 368–371.

(17) Van Zee, R. J.; Ferrante, R. F.; Zeringue, K. J.; Weltner, W. Jr. *J. Chem. Phys.* **1981**, *75*, 5297–5299.

(18) Longuet-Higgins, H. C. *J. Chem. Phys.* **1950**, *18*, 265–274.

(19) Borden, W. T.; Davidson, E. R. *J. Am. Chem. Soc.* **1976**, *99*, 4587–4594.

(20) Ovchinnikov, A. A. *Theoret. Chim. Acta (Berl.)* **1978**, *47*, 297; Ovchinnikov, A. A.; Misurkin, I. A. *Russ. Chem. Rev. (Eng. Transl.)* **1977**, *46*, 967–987.

(21) Klein, D. J.; Nelin, C. J.; Alexander, S.; Matsen, F. A. *J. Chem. Phys.* **1982**, *77*, 3101–3108.

(22) Klein, D. J. *Pure Appl. Chem.* **1983**, *55*, 299–306, and private communication.

(23) Lieb, E.; Mattis, D. *J. Math. Phys.* **1962**, *3*, 749–751.

(24) Anderson, P. W. *Phys. Rev.* **1961**, *124*, 41–52; Friedel, J. *Canad. J. Phys.* **1956**, *34*, 1190; *Nuovo. Cimento Suppl.* **1958**, *2*, 287.

(25) Mataga, N. *Theor. Chim. Acta* **1968**, *10*, 372–376.

(26) Itoh, K. *Bussei* **1971**, *12*, 635–646.

(27) Tyutyulkov, N.; Schuster, P.; Polansky, O. E. *Theor. Chim. Acta* **1983**, *63*, 291–304. Tyutyulkov, N.; Polansky, O. E.; Schuster, P.; Karabunarliev, S.; Ivanov, C. I. *Theor. Chim. Acta* **1985**, *67*, 211–228. Tyutyulkov, N. N.; Karabounarliev, S. H. *C. R. Acad. Bulg. Sci.* **1985**, *38*, 79–81.

(28) Nasu, K. *Phys. Rev. B: Solid State* **1986**, *B33*, 330–338.

(29) Rosinski, C.; Elschner, B. *J. Magn. Magn. Mater.* **1977**, *4*, 193–198.

(30) Birgeneau, R. J.; Dingle, R.; Hutchings, M. T.; Schirane, G.; Holt, S. L. *Phys. Rev. Lett.* **1971**, *26*, 718–721. Dietz, R. E.; Merritt, F. R.; Dingle, R.; Daniel, H.; Silbernagel, B. G.; Richards, P. M. *Ibid.* **1971**, *26*, 1186–1188.

(31) Shimizu, M.; Ajiro, Y. *J. Chem. Phys.* **1982**, *76*, 1273–1278.

(32) Steiner, M.; Villain, J.; Windsor, C. G. *Adv. Phys.* **1976**, *25*, 87–209.

(33) McConnell, H. *Proc. R. Acad. Welch Found. Conf.* **1967**, *11*, 144.

(34) Breslow, R.; Jaun, B.; Kluttz, R. Q.; Xia, C. Z. *Tetrahedron* **1982**, *38*, 863–867.

(35) Breslow, R.; Maslak, P.; Thomaidis, J. S. *J. Am. Chem. Soc.* **1984**, *106*, 6453–6454.

3-Methylisophthalophenone-3'-carboxylic Acid. To a hot solution of 30.8 g (0.10 mol) of 3,3'-dimethylisophthalophenone in 900 mL of acetic acid was added with stirring 432 g (1.65 mol) of sodium dichromate in small portions. After the addition, the mixture was refluxed for 70 h. Most of the solvent was removed by distillation, and the mixture was made alkaline with aqueous sodium hydroxide. The precipitate was removed by filtration, and the filtrate was acidified with aqueous hydrochloric acid. The new precipitate was collected and dried to give 34.4 g (100%) of colorless crystals: mp 321–326 °C; IR ν_{OH} 3150–2100 cm^{-1} , ν_{CO} 1690, 1660 cm^{-1} ; $^1\text{H NMR}$ (CDCl_3) δ 2.48 (s, 3 H), 7.44–8.48 (m, 12 H).

Isophthalophenone-3,3'-dicarboxylic Acid. To a hot suspension of 10 g (0.029 mol) of the monocarboxylic acid in 200 mL of aqueous potassium hydroxide was added in small portions 18.3 g (0.116 mol) of potassium permanganate. After the addition, the mixture was refluxed for 1.5 h. After cooling, the mixture was acidified with dilute sulfuric acid. Manganese dioxide was dissolved by a dropwise addition of hydrogen peroxide. The white precipitate was collected, dissolved in aqueous sodium hydroxide, and reprecipitated by hydrochloric acid: mp 328–334 °C; 8.7 g (80%); IR ν_{OH} 3200–2500 cm^{-1} , ν_{CO} 1690, 1660 cm^{-1} .

3,3'-Dibenzoylisophthalophenone. A mixture of 7.91 g (0.021 mol) of the dicarboxylic acid and 70 mL of thionyl chloride was heated to a gentle reflux for 8 h under exclusion of moisture. The excess thionyl chloride was distilled off. The bis(acid chloride) was obtained as a light-brown residue (8.6 g, 100%) (IR 1755, 1600 cm^{-1}) and used without purification for the following reaction. A solution of 15.1 g (0.037 mol) of the bis(acid chloride) in 200 mL of dry benzene was added dropwise at 0 °C to a suspension of 24.5 g (0.184 mol) of anhydrous aluminum chloride in 300 mL of dry benzene. The mixture was allowed to warm to room temperature and stirred for 3 h. The mixture was poured onto ice-water containing hydrochloric acid and the organic layer was separated. The remaining solid was dissolved in chloroform. The two organic solutions were washed separately with water and aqueous sodium hydroxide and dried over magnesium sulfate. The crystals obtained after evaporation of the solvents were combined and recrystallized from benzene-hexane (1:2) to give 15.3 g (78%) of colorless prisms: mp 219–219.5 °C; IR ν_{CO} 1660 cm^{-1} ; $^{13}\text{C NMR}$ (CDCl_3) δ 137.1, 137.4, 137.6, 138.2 (quaternary carbons), 195.0, 195.9 (carbonyl carbons). Anal. Calcd for $\text{C}_{37}\text{H}_{22}\text{O}_4$: C, 82.58; H, 4.48. Found: C, 82.63; H, 4.36.

3,3'-Dibenzoylisophthalophenone Tetrahydrazone. A mixture of 2.0 g (3.8 mmol) of the tetraketone and 50 mL of hydrazine hydrate in 250 mL of ethanol was heated under reflux for 40 h. The solvent was evaporated, and the residue was dissolved in benzene. Pale-yellow crystals were precipitated by addition of petroleum ether: 1.8 g (79%); IR 3360, 3260, 3190, 1610, 1575, 1555 cm^{-1} ; $^1\text{H NMR}$ (CDCl_3) δ 5.10–5.80 (br s, 8 H, exchangeable with D_2O), 7.30–7.73 (m, 22 H aromatic).

***m*-Phenylenebis[*m*-(α -diazobenzyl)phenyldiazomethane] (2).** To a stirred solution of the tetrahydrazone (0.50 g, 0.91 mmol) in 120 mL of dry ether were added 1.8 g (0.02 mol) of active manganese dioxide (Merck, 5953 activated granular) and a few drops of saturated ethanolic potassium hydroxide in the dark. The reaction was monitored by measuring the growth of the IR absorption at 2040 cm^{-1} due to the diazo group of the aliquots. The absorbance became maximum at 1.5 h, when the mixture was filtered. The wine-red solution was concentrated to a few milliliters under reduced pressure to give 220 mg (45%) of purple crystals: mp 113 °C dec; IR ν_{NN} 2040 cm^{-1} ; $^1\text{H NMR}$ (400 MHz) (CDCl_3) δ 7.09 (d of t, 6 H, $J = 7.9, 1.4$ Hz, 4,6-H of 1,3-disubstituted rings), 7.18 (m, 5 H, 2-H of 1,3-disubstituted rings and *p*-H of terminal rings), 7.28 (d of m, 4 H, $J = 7.7$ Hz, *o*-H of terminal rings), 7.38 (t, 4 H, $J = 7.7$ Hz, *m*-H of terminal rings), 7.39 (t, 3 H, $J = 7.9$ Hz, 5-H of 1,3-disubstituted rings); UV λ_{max} (log ϵ) 249 (4.91), 5.18 nm (2.65). Anal. Calcd for $\text{C}_{34}\text{H}_{22}\text{N}_8$: C, 75.26; H, 4.09; N, 20.65. Found: C, 75.10; H, 4.00; N, 20.50.

B. Sample Preparation. Benzophenone was chosen as a host molecule because its crystal was found to incorporate well the diazo precursor **2** in spite of their large difference in molecular size. Its crystal structure has been determined by X-ray diffraction,³⁶ the space group being $P2_12_12_1$ with $Z = 4$. Benzophenone was purified by repeated recrystallizations from ethanol. Some crystals were further zone-refined but showed no appreciable effect on ESR spectra. Single crystals of benzophenone containing **2** as a guest were obtained as follows. A benzene-ethanol (1:6) mixed solution containing 0.00130 mol fraction of **2** in benzophenone was prepared at temperatures slightly below 20 °C. Single crystals were grown in the dark by slowly cooling the mixed solution in a thermostated bath, the temperature gradient being 0.2–0.3 °C per day. Light-red crystals of a desired size in the rectangular form

were obtained from the wine-red mixed solution. The actual concentration of **2** in single crystals was determined by means of UV spectra; the typical value was 5×10^{-4} mol/dm³ of the single crystal. The size of the single crystals was typically 1.5 × 3 × 8 mm and 1 × 2 × 3 mm for X-band and K-band experiments, respectively.

C. Electron Spin Resonance Measurements. The single crystal was mounted on a Teflon wedge or sample holder in an ESR cavity in such a manner that the static magnetic field H_0 rotates in the crystallographic plane of the host crystal. The nonet hydrocarbon **1** was formed at 4.2 K by photolysis of **2** in the crystal with the 405-nm line from an XBO 500-W high-pressure mercury lamp (OSRAM) equipped with a glass filter (Toshiba UV39) and a 5-cm solution filter of 100 g of $\text{CuSO}_4 \cdot 5\text{H}_2\text{O}/\text{dm}^3$. For measurements of photochemical reaction rates, light intensity was adjusted by means of neutral density filters (Toshiba) which transmitted 5.4, 9.2, 21.0, and 30.0% of the 405-nm line from the mercury lamp.

ESR measurements were carried out at both X-band and K-band microwave frequencies. We used a JEOL-3BX ESR spectrometer equipped, for the X-band ESR, with a microwave unit (JEOL-ESSCX) and a homemade TE_{102} rectangular cavity ($Q = 6800$ at 4.2 K) operating between 9.5 and 9.6 GHz and, for the K-band ESR, with a microwave unit (JES SK) and a homemade TE_{011} cylindrical cavity ($Q = 12000$ at 4.2 K) operating between 25.0 and 26.0 GHz. The microwave oscillating field H_1 lies in the same plane as H_0 at the X band, the angle between H_0 and H_1 being a function of the magnet rotation, while at the K band H_1 was always perpendicular to H_0 .

The angular dependence of the ESR spectra was measured by rotating the magnet. Because the nonet spectra sharply changed with rotation of the magnetic field, the single crystal was mounted with the aid of a polarizing microscope in order to obtain as good a precision as possible. The direction of the crystal axes was determined to 0.2° accuracy from the crossing point of the resonance lines arising from the two magnetically nonequivalent sites in the crystal. When only one site was detected in the K-band experiment, an X-irradiated single crystal of L-cystine (C2 space group) was also mounted on the same wedge and its signals were utilized as a reference for determining the crystal axes of the sample crystal. The total error in defining the direction of the magnetic field with respect to the crystal axes was estimated to be within 1.5°.

The temperature dependence of the ESR spectra was observed in the range 1.8–160 K at the X band and 4.2–160 K at the K band. Chromium(III) in MgO powder was adopted as a reference substance for intensity measurements. The sample temperature above 4.2 K was measured with the chromel P-constantan thermocouple attached to the outside wall of the cavity. The experiment below 4.2 K was done by pumping liquid helium, and the temperature was obtained from the helium vapor pressure.

Results and Analyses

A. Synthesis of *m*-Phenylenebis[*m*-(α -diazobenzyl)phenyldiazomethane] (2). A synthetic route similar to that employed for tridiazocompounds³⁷ was first tried. Since bromination of isophthalophenone (27%) and the replacement of the aromatic bromo substituent with the cyano group (44%) were not very efficient and required tedious workup, we opted for a different route. The Grignard reagent from *m*-bromotoluene was allowed to react with isophthalonitrile. 1,3-Di-(*m*-toluoyl)benzene was obtained in 80% yield after acid hydrolysis. The methyl group was oxidized in two steps, first with sodium dichromate in boiling acetic acid to the monocarboxylic acid and second with potassium permanganate in aqueous potassium hydroxide to isophthalophenone-3,3'-dicarboxylic acid in high yield. The Friedel-Crafts reaction of the bis(acid chloride) in benzene gave 3,3'-dibenzoylisophthalophenone. The tetrahydrazone was obtained by the reaction of the tetraketone with excess hydrazine hydrate in ethanol and oxidized with active manganese dioxide in ether to the tetradiazocompound obtained as purple crystals.

The above reactions are all straightforward and leave no doubt that the structures are correct. Furthermore, the connectivity of the backbone was confirmed by the $^{13}\text{C NMR}$ spectrum of the tetraketone. It shows two carbonyl carbon signals of equal intensity at δ 195.0 and 195.9. The NMR of the triketone shows two carbonyl signals of 1:2 relative intensity at δ 195.2 and 195.9, respectively.³⁷ By comparison, the tetraketone has two inner (δ 195.0) and two outer (δ 195.9) carbonyl groups along the mo-

(36) Fleischer, E. B.; Sung, N.; Hawkinson, S. *J. Phys. Chem.* **1968**, *72*, 4311–4312.

(37) Teki, Y.; Takui, T.; Nakatoh, K.; Itoh, K.; Iwamura, H.; Kobayashi, K., unpublished results.

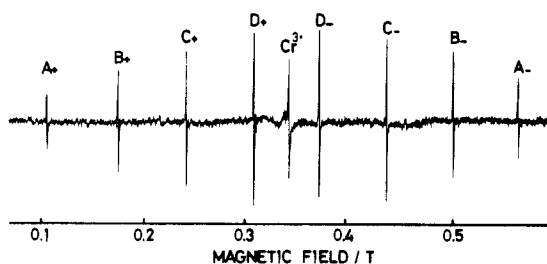
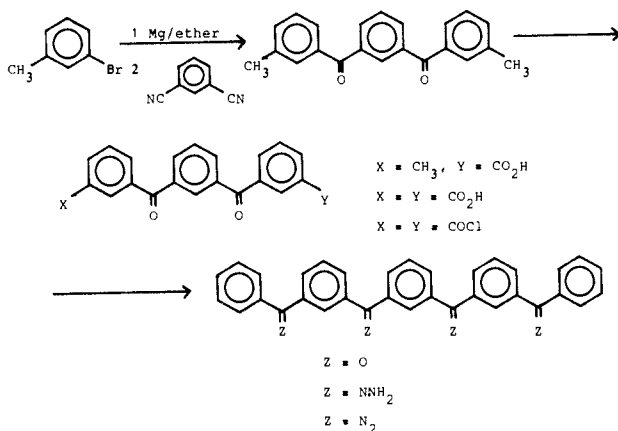


Figure 1. X-band ESR spectrum observed after photolysis at 4.2 K with the magnetic field along the direction 26° from the a axis in the ab plane of the host crystal. The microwave frequency ν is 9550.6 MHz. The central line is due to Cr^{3+} in the MgO powder used as a reference substance.

lecular chain. There are four quaternary ring carbons of nearly equal intensity. These spectral data are uniquely consistent with the regular chain structure of the tetraketone, with an effective symmetry plane going through the middle benzene ring.



B. Features of the X-Band ESR Spectra at 4.2 K. ESR spectra were observed in the absorption mode at X band. It was found that in order to avoid saturation, the microwave power level should be attenuated to as low as $0.5 \mu\text{W}$ because of the long spin-lattice relaxation time of **1** at liquid helium temperature. An 80-Hz field modulation was employed for the purpose of suppressing the rapid passage effect³⁸ on the ESR transitions and obtaining accurate line shapes and absorption intensities.

Figure 1 shows the typical ESR spectrum observed at 4.2 K after photolysis. The spectrum consists of four well-resolved pairs A_\pm , B_\pm , C_\pm , and D_\pm ; the relative separations of each pair are nearly $(A_- - A_+)/ (B_- - B_+)/ (C_- - C_+)/ (D_- - D_+) = 7:5:3:1$ and the relative integrated intensities are nearly $A_\pm/B_\pm/C_\pm/D_\pm = 4:7:9:10$. These ratios are just what one would expect for the $\Delta M_S = \pm 1$ allowed transitions between the fine-structure sublevels of the nonet spin manifold in the high-field limit. The assignment of the transitions to the magnetic quantum number M_S is $A_\pm (\pm 4 \leftrightarrow \pm 3)$, $B_\pm (\pm 3 \leftrightarrow \pm 2)$, $C_\pm (\pm 2 \leftrightarrow \pm 1)$, and $D_\pm (\pm 1 \leftrightarrow 0)$. Figure 2 shows the observed angular dependence of these four pairs. When the magnetic field is applied in the crystallographic ab plane, there are two magnetically nonequivalent sites in the benzophenone crystal owing to the orthorhombic symmetry. Figure 1 shows, however, only one set of nonet signals. This indicates that only one of the two nonequivalent sites is selectively occupied by the guest molecule (see the next section).

From the angular dependence of the resonance fields, the spin-Hamiltonian parameters could be evaluated from the third-order perturbation theory. However, it was difficult to obtain from the X-band experiment accurate enough parameters to reproduce satisfactorily the observed spectra: the perturbation treatment is no longer justified for the lower field transitions on account of the small Zeeman energy which is taken as the unperturbed Hamiltonian. Therefore, the K-band experiment was

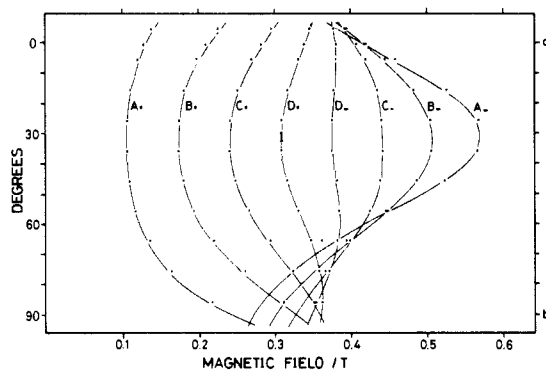


Figure 2. Angular dependence of the X-band resonance fields of the eight allowed transitions for **1** observed at 4.2 K for rotation of the magnetic field in the ab plane ($\nu = 9550.2$ MHz). The solid points represent the observed values and the solid curves the calculated ones. A_\pm , B_\pm , C_\pm , and D_\pm correspond to the transitions $M_S = \pm 4 \leftrightarrow \pm 3$, $\pm 3 \leftrightarrow \pm 2$, $\pm 2 \leftrightarrow \pm 1$, and $\pm 1 \leftrightarrow 0$, respectively.

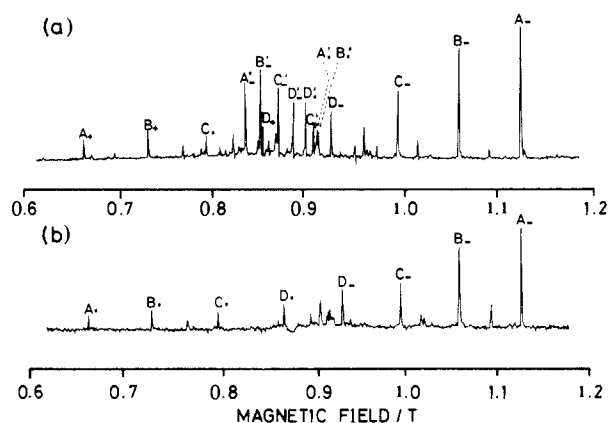


Figure 3. K-band ESR spectra observed after photolysis at 4.2 K with the magnetic field along the direction 30° from the a axis in the ab plane. (a) The two sets of signals arising from the magnetically nonequivalent sites were observed ($\nu = 25069.7$ MHz). (b) Only one set of signals was observed ($\nu = 25125.4$ MHz).

undertaken to overcome this difficulty.

C. Features of the K-Band ESR Spectra at 4.2 K. For the sake of high sensitivity at very low microwave power levels, we have employed a 100-kHz field modulation at the K band and we have recorded the spectra in the dispersion mode at the expense of the accurate line shape. Figure 3 shows two typical K-band ESR spectra observed at 4.2 K in nearly the same orientation of the magnetic field as in Figure 1, i.e., along a direction 30° from the a axis in the ab plane. This direction is nearly coaxial with the principal Z axis of the fine structure tensor as shown in the next section. The spectrum in Figure 3a consists of two sets of eight lines distinguished by primed and unprimed symbols. These sets originate from sites magnetically nonequivalent with each other with respect to the magnetic field in the ab plane because their angular dependence obeys orthorhombic symmetry. On the other hand, only one of the two sets is seen in Figure 3b, similarly to the case of the X-band spectrum in Figure 1. These features depend on the sample. The two crystals giving rise to the spectra shown in spectra a and b in Figure 3 were cut from the same crystal and correspond, respectively, to the middle and the end of a rectangular crystal elongated along the c axis. This indicates that the choice of particular sites by the guest molecules is sensitive to the conditions of crystal growth.

The angular dependence of the resonance fields of the spectra in Figure 3a is shown in Figure 4 with the magnetic field applied in the ab plane. This clearly shows that the ratio of the relative separations mentioned above holds for all the directions of the magnetic field. The same ratio was also observed in the other two crystallographic planes. On the other hand, contrary to the X-band experiment, noticeable deviation from the expected in-

(38) Weger, M. *Bell Syst. Technol. J.* **1960**, *39*, 1013-1112.

Table I. Hamiltonian Parameters g , D , and E and the Fine-Structure Tensors for the Isomers I-IV^a

isomer	g	D , cm ⁻¹	E , cm ⁻¹	principal axes	principal values, cm ⁻¹	direction cosines		
						a	b	c
I	2.002	0.031 61	-0.003 94	X	-0.014 48	0.290 16	-0.594 91	0.749 56
				Y	-0.006 60	-0.472 96	0.591 80	0.652 76
				Z	0.021 07	0.831 94	0.543 93	0.109 65
II (64 K)	2.002	0.032 27	-0.002 25	X	-0.013 01	0.377 41	-0.715 15	0.588 32
				Y	-0.008 51	-0.428 14	0.428 58	0.795 62
				Z	0.021 51	0.821 13	0.552 16	0.144 43
III (64 K)	2.002	0.033 47	-0.002 16	X	-0.013 32	0.627 76	-0.778 40	0.003 72
				Y	-0.009 00	-0.112 69	-0.086 15	0.989 89
				Z	0.022 31	0.770 21	0.621 83	0.141 80
IV (92 K)	2.002	0.032 41	-0.004 03	X	-0.014 83	0.297 80	-0.608 64	0.735 44
				Y	-0.006 77	-0.466 40	0.579 43	0.668 38
				Z	0.021 61	0.832 94	0.542 06	0.111 31

^a The direction cosines are referred to the crystallographic axes for $P2_12_12_1$. The signs of the direction cosines for the isomer I correspond to the unprimed set in Figure 3.

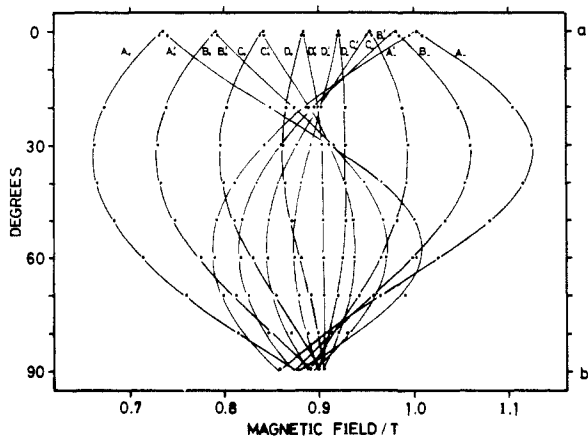


Figure 4. Angular dependence of the K-band resonance fields of the allowed transitions observed at 4.2 K for rotation of the magnetic field in the ab plane ($\nu = 25069.7$ MHz). The solid points represent the observed values and the solid curves the calculated ones. The primed pairs A_{\pm}' , B_{\pm}' , C_{\pm}' , and D_{\pm}' and the unprimed pairs A_{\pm} , B_{\pm} , C_{\pm} , and D_{\pm} arise from the two magnetically nonequivalent sites occupied by the nonet hydrocarbons.

tensity relationship (4:7:9:10:10:9:7:4) characterizes the K-band experiments as shown in Figure 3. This deviation is a manifestation of the Boltzmann distribution which affects the K band because of the large Zeeman splittings compared with those of the X band. It serves to determine the absolute sign of the fine-structure parameter D as discussed in the next section.

D. Analysis of the Spectra at 4.2 K. The angular dependence of the resonance fields and of the signal intensities of the eight lines described above was well-reproduced by the spin Hamiltonian

$$\begin{aligned} \mathcal{H} &= \beta \cdot \mathbf{H} \cdot \mathbf{g} \cdot \mathbf{S} + \mathbf{S} \cdot \mathbf{D} \cdot \mathbf{S} \\ &= \beta \cdot \mathbf{H} \cdot \mathbf{g} \cdot \mathbf{S} + D[S_z^2 - S(S+1)/3] + E(S_x^2 - S_y^2) \end{aligned} \quad (1)$$

with $S = 4$. The first term represents the electronic Zeeman Hamiltonian and the others stand for the fine-structure Hamiltonian. Here, \mathbf{g} is the g tensor and \mathbf{D} the fine-structure tensor which is diagonal with $D_{XX} = -D/3 + E$, $D_{YY} = -D/3 - E$, and $D_{ZZ} = 2D/3$. Higher order terms in \mathbf{S} which are group theoretically allowed for $S = 4$ ³⁹ were found to be negligibly small. The analysis of the spectra observed at the K band was carried out by means of a third-order perturbation calculation based on the spin Hamiltonian (eq 1), the fine-structure terms being the perturbation Hamiltonian. The expressions for the resonance fields to third order and for the relative transition intensities to second order are given in the Appendix.¹³

The g value, the fine-structure parameters, and the direction cosines of the principal axes of the fine-structure tensor were

accurately determined by the least-squares method and are listed in the first row of Table I. For each case, the root mean square (rms) of the difference between the calculated and observed resonance fields is less than 1×10^{-3} T, which is within the line width. The g value is isotropic within experimental error and close to the free spin value of 2.0023. The absolute sign of the fine-structure parameter D was easily and unequivocally determined as positive from the effect of the Boltzmann distribution described in the preceding section: The absolute sign of the g value, which determines the sequence of the Zeeman levels, is positive because the free spin value is positive; moreover g values of orbital singlets are known to be positive. The unprimed set in Figure 3 corresponds to the spectrum with the magnetic field only 7° away from the principal Z axis as easily obtained from the direction defined in the caption and the direction cosines for I given in Table I. In this direction, D_0 in the Appendix is very nearly the negative of the Z principal value $-D_{ZZ} = -2D/3$. Therefore, the resonance fields of A_{\pm} are approximately given by $H_0 \mp (21/2g\beta)D_{ZZ} \approx H_0 \mp 7D/g\beta$ from eq A1 in the Appendix. Since the energy levels associated with A_+ ($+4 \leftrightarrow +3$) lie higher than those associated with A_- ($-3 \leftrightarrow -4$) for $g > 0$ and $g\beta H_0 \gg 7|D|$ for K-band spectra, only the positive D value accounts for the fact that A_+ appearing on the low-field side of the spectrum was weaker than A_- .

From the parameters given in Table I, the resonance fields at the K band were calculated by using eq A1-A4, and they are shown with the solid curves in Figure 4. On the other hand, the resonance fields of the X-band spectra were computed by exact numerical diagonalization of the spin Hamiltonian (eq 1). They are shown in Figure 2 by the solid curves; note that the perturbation approximation is invalid at low magnetic fields below 0.2 T. The quite satisfactory agreement between the calculated and observed values (Figures 2 and 4) proves undoubtedly the photochemically generated hydrocarbon **1** to be in the nonet state. It should be mentioned that the observed fine structure and its angular dependence could not be interpreted by any superposition of the spectra of more than one paramagnetic species with $S = 1, 2$, and 3.

E. Spin Multiplicity of the Lowest Energy Level. For a system with eight unpaired electrons, five kinds of energy levels with $S = 0, 1, 2, 3$, and 4 are permissible. We have already shown that the hydrocarbon **1** occupies a nonet energy level. It remains to find the location of the other levels and to ascertain whether the nonet level is the lowest. Figures 1 and 3 show that the ESR spectra of the nonet state only were observable at 4.2 K. Moreover, no triplet, quintet, and septet signals could be detected up to the temperature where **1** decomposed, i.e., 160 K. Given the sensitivity of the spectrometer, it can therefore be concluded that the spin states other than the singlet (which is undetectable by ESR) are located at least 300 cm⁻¹ above the nonet state.

As to the singlet state, one can estimate its location from the temperature dependence of the total intensity of the nonet signals, $I_4(T)$. Since the populations of the excited triplet, quintet, and septet states are negligible even at 160 K, one may limit consideration to a singlet-nonnet system with an energy separation ΔE .

(39) Abragam, A.; Bleaney, B. "Electron Paramagnetic Resonance of Transition Metals"; Clarendon Press: Oxford, 1970; p 341.

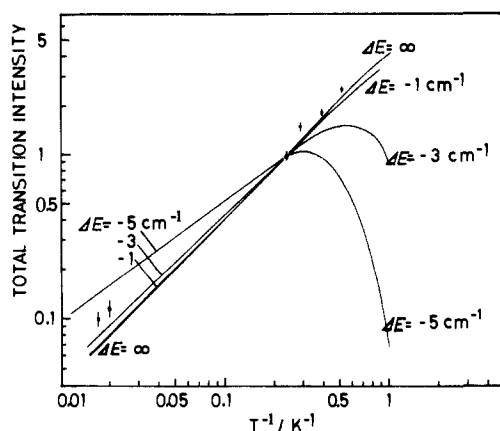


Figure 5. Plots of the total signal intensities for the nonet isomer I as a function of inverse temperature. The solid points and the vertical lines represent the experimental values and their errors, respectively, and the solid curves the calculated values. The energy separation between the singlet and nonet states is ΔE .

If the energy of the spin sublevels in the nonet state is denoted by E_m and the energy of the singlet state by E_S , the total intensity of the nonet signals at a given temperature, $I_4^{\text{calcd}}(T)$, can be calculated from eq 2–5 where $N(T, m, m+1)$ is the Boltzmann

$$I_4^{\text{calcd}}(T) = A \sum_m |(m+1)S_z| |m\rangle|^2 N(T, m, m+1) \quad (2)$$

$$N(T, m, m+1) = |\xi_m(H_m) - \xi_{m+1}(H_m)| / [\sum_i \xi_i(H_m) + \xi_S] \quad (3)$$

$$\xi_m(H_m) = \exp[-(E_m - E_0)/kT] \quad (4)$$

$$\xi_S = \exp[-(E_S - E_0)/kT] \quad (5)$$

factor and A is a constant to normalize to unity the total intensity at 4.2 K. The sum runs over the nonet spin manifold. The energy E_0 represents the lowest level among the E_m 's and E_S . It should be noted that the resonance field H_m for the $|m\rangle \leftrightarrow |m+1\rangle$ transition is different for different m 's under the constant $h\nu$. Thus, even if $\Delta E \gg kT$, the ESR total intensity $I_4^{\text{calcd}}(T)$ vs. $1/T$ plot does not obey simply Curie's law, unlike the static magnetic susceptibility.

We measured the absorption intensities at the X band in the range 1.8–56 K using the 80-Hz field modulation in order to detect the nonet signals in the absorption mode free from the rapid passage effect³⁸ at very low temperature. To compensate various temperature factors which contribute to the spectrometer sensitivity, the observed total intensity, $I_4(T)$, was calibrated with Cr^{3+} in MgO powder ($S = 3/2$) by using⁴⁰

$$I_4(T) = [I_{3/2}^{\text{calcd}}(T)/I_{3/2}(T)] \sum_m I_4(T, m, m+1) \quad (6)$$

where

$$I_{3/2}^{\text{calcd}}(T) = \sum_{m'} I_{3/2}^{\text{calcd}}(T, m', m'+1) \quad (7)$$

$$I_{3/2}(T) = \sum_{m'} I_{3/2}(T, m', m'+1) \quad (8)$$

Here $I_{3/2}(T, m, m+1)$ and $I_4(T, m, m+1)$ are the observed integrated intensity of the $|m\rangle \leftrightarrow |m+1\rangle$ transitions for Cr^{3+} and the nonet molecule, respectively and $I_{3/2}^{\text{calcd}}(T, m, m+1)$ is the calculated intensity for Cr^{3+} in an arbitrary unit. This substance is excellent as a reference for signal intensity from the following reasons. First, $\text{Cr}^{3+}(^4F_{3/2})$ in the cubic field of MgO is an orbital singlet with $S = 3/2$, and the powder spectrum is simply a single line at $g = 1.9797$ ⁴¹ as shown in Figure 1. Second, since its excited states are located so high relative to kT that their Boltzmann population is quite negligible,⁴¹ $I_{3/2}(T)$ can be exactly calculated within the ground-state spin manifold.

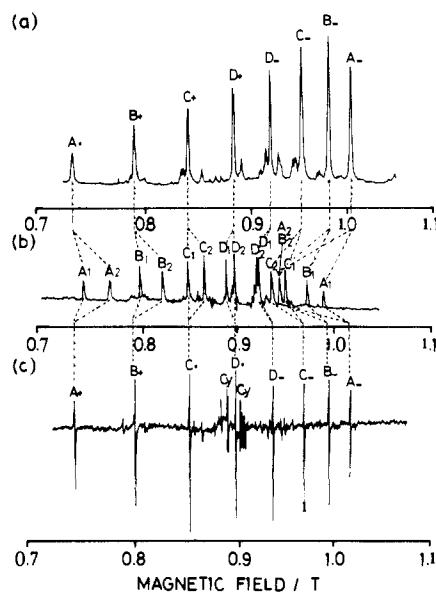


Figure 6. Temperature dependence of the K-band ESR spectrum with the magnetic field along the a axis. (a) The spectrum observed in the dispersion mode at 4.2 K after photolysis and before the conformational change ($\nu = 25069.7$ MHz). (b) The spectrum observed in the dispersion mode at 77 K after the first conformational change at 64 K ($\nu = 25145.9$ MHz). (c) The spectrum observed in the absorption mode at 77 K after completing the second conformational change at 92 K ($\nu = 25443.6$ MHz). The symbol Cy indicates the reference signal of an X-irradiated single crystal of L-cystine dihydrochloride.

The corrected total signal intensity is plotted as the points in Figure 5 vs. inverse temperature, the value at 4.2 K being normalized to unity. The solid curves are plots of the total intensity calculated based on eq 5 for $\Delta E = -5, -3, -1$, and $+\infty$ in inverse centimeters, where ΔE is given by the energy separation between E_S and the mean of E_m 's and positive when the ground state is nonet. If the singlet state was located below the nonet state ($\Delta E < 0$), a considerable decrease in the total intensity would occur below 4.2 K. However, since the plot of the observed values shows no appreciable decrease as indicated in Figure 5, it is safely concluded that the observed nonet state is the electronic ground state.

F. Isomers Caused by Thermally Activated Conformational Changes. When the sample was warmed from 4.2 K, the K-band ESR spectrum in Figure 6a changed remarkably at 64 K into a complicated one (Figure 6b). The new spectrum is the superposition of the spectra for two magnetically different molecules both in the nonet state. We designate these as isomers II and III. Isomer I is the nonet molecule observed at 4.2 K after photolysis. As the temperature was further raised, the spectrum showed another change at 92 K and became that shown in Figure 6c, due to another nonet molecule, isomer IV. These changes were irreversible; the spectra of isomers II, III, and IV remained unchanged when the sample was again cooled down to 4.2 K.

In order to determine the spin Hamiltonian parameters in eq 1, the angular dependence of the K-band resonance fields of isomers II–IV was measured at 77 K. We used the spectrum due to only one of the two nonequivalent sites in the crystal because the spectrum due to the other site was weak. The results in the ab plane are shown in Figure 7 (isomers II and III) and Figure 8 (isomer IV); the points are the observed values. The spectra shown in Figure 6b and 6c correspond to the angle 0° in the ordinates of Figures 7 and 8, respectively. The Hamiltonian parameters experimentally determined by the least-squares method are summarized in Table I. The absolute signs of D for isomers II–IV are also positive; they are obtained by the same method as for isomer I.

The solid curves in Figures 7 and 8 are plots of the resonance fields calculated from the parameters in Table I using eq A1–A4 for $S = 4$. The excellent agreement with the observed values indicates that all the isomers are in their nonet states. In addition,

(40) Takui, T. Dr. Thesis, Osaka University, 1973.

(41) Wertz, J. E.; Auzins, P. *Phys. Rev.* **1957**, *106*, 484.

Table II. Comparison of D , E , and $(2S - 1)D$ (in cm^{-1}) with Those of the Known High-Spin Hydrocarbons with Similar Electronic Structures

hydrocarbons	S	D	$ E $	$(2S - 1)D$	ref
diphenylmethylene	1	0.405 05	0.019 18	0.4050	42
<i>m</i> -phenylenebis(phenylmethylene)	2	0.071 31	0.019 02	0.2139	7
benzene-1,3,5-tris(phenylmethylene)	3	0.041 58	0.010 26	0.2079	10
3,3'-diphenylmethylenebis(phenylmethylene)	3	0.048 74	0.008 89	0.2437	13
<i>m</i> -phenylenebis[(diphenylmethylene-3-yl)methylene] isomer I	4	0.031 61	0.003 94	0.2213	
isomer II	4	0.032 27	0.002 25	0.2260	this work
isomer III	4	0.033 47	0.002 16	0.2343	
isomer IV	4	0.032 41	0.004 03	0.2269	

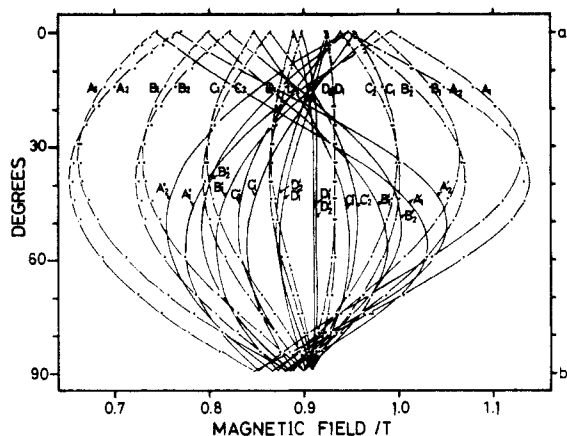


Figure 7. Angular dependence of the K-band resonance fields of the allowed transitions of nonet isomers II and III resulting from the conformational change at 64 K. The resonance fields were observed at 77 K ($\nu = 25\,145.9$ MHz). The solid points represent the observed values and the solid curves the calculated ones. The subscripts 1 and 2 indicate the isomers II and III, respectively. Only one set of the signals with stronger intensities is plotted by the solid points.

the nonet states for isomers II–IV are the ground state. This conclusion was drawn, in a similar manner as for I, by measuring the intensity as a function of temperature. The observed fine-structure tensors differ from isomer to isomer (Table I). These thermal changes are conformational changes, to be discussed in detail in a later section.

G. Evidence of a One-Photon Process in the Photodissociation into the Nonet Hydrocarbon 1. Since the diazo precursor **2** has four diazo groups, one might expect partial photodissociation of **2** to lead to various intermediates. However, as described in section E, only the nonet hydrocarbon **1** was observed after photolysis at 4.2 K. Moreover, the ESR spectrum of **1** appeared as soon as the UV irradiation started, and regardless of the light intensity, no spectra due to other paramagnetic species were observed throughout photolysis until the reaction was completed. These findings suggest that **1** was formed from **2** not by stepwise release of successive nitrogen molecules but rather by a direct process, involving possibly a single photon in the host single crystal. To test this hypothesis, the dependence of the photochemical reaction rates on light intensity was measured by single-crystal ESR.

Photolysis was made in the ESR cavity at 4.2 K, the incident light path being along the c axis of the benzophenone crystal. The ESR intensity was measured at the X band for the magnetic field along the direction 2.9° away from the b axis in the bc plane with the 80-Hz field modulation. Initially the ESR intensity (or relative yield Y) increased linearly with the irradiation time and tended to saturate gradually. Because of the dilute concentration of the doped diazo precursor **2** and because of its low absorbance at 405 nm, we can safely assume a first-order kinetics for its photodissociation. Thus, the relative reaction rate k at time t was obtained by extrapolating the linear portion of the Y plots to time zero, because $[1]/[2]_{t=0} \approx kt$ for $kt \ll 1$. Dependence of the observed k on the light intensity I was fitted to $k = cI^n$, with a constant c yielding a value for $n = 1.02$. This result indicates a highly efficient photodissociation of **2** in benzophenone crystals: this process required just one photon. Other details of the photochemical reaction will be published elsewhere.

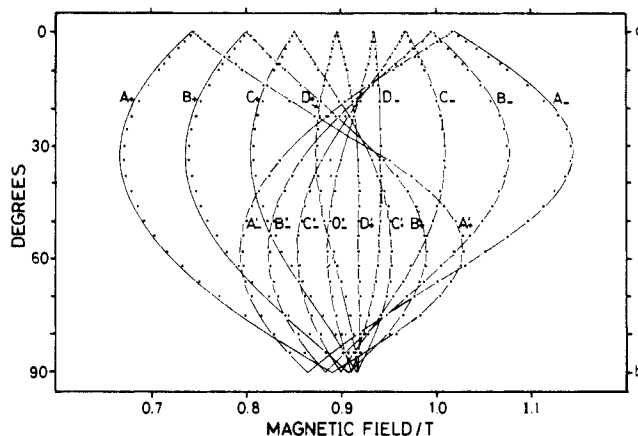


Figure 8. Angular dependence of the K-band resonance fields of the allowed transitions of the nonet isomer IV resulting from the conformational change at 92 K. The resonance fields were observed at 77 K ($\nu = 25\,443.6$ MHz). The solid points represent the observed values and the solid curves the calculated ones.

Discussion

A. g Value and the Fine-Structure Parameters. Table I shows that the g values of all four nonet isomers are nearly isotropic and close to the free spin value of 2.0023. This indicates a small spin-orbit interaction in these paramagnetic species: both the anisotropy of g values and a shift from the free spin value are proportional to the spin-orbit coupling constants of the constituent atoms.^{43,44} The small spin-orbit interaction and the negligible contribution from orbital angular momentum are also indicated by the absence of the fine-structure terms higher than quadratic in S , which are predominantly due to the spin-orbit coupling as could be estimated from a perturbation approach to the spin Hamiltonian.^{39,45} This is important support for photochemical generation of hydrocarbon **1**, as the hydrogen and carbon atoms have very small spin-orbit coupling constants.

The observed fine-structure parameters of the four isomers are $D = 0.031\,61 \sim 0.033\,47$ cm^{-1} and $E = -0.002\,16 \sim -0.004\,03$ cm^{-1} , the ratio E/D being $-0.0645 \sim -0.1246$. Table II compares these values with those of the known high-spin hydrocarbons with similar electronic structures. Since D decreases apparently with increasing S , one might infer this to result from the larger size of the molecules with the larger S , in which the average spin-spin distance is long. Actually, this is not true, in contrast to $\pi\pi^*$ triplet states. If we compare $(2S - 1)D$ instead of D for the high-spin hydrocarbons with $S \geq 2$, this quantity assumes nearly a constant value between 0.2 and 0.25 (Table II). For the high-spin hydrocarbons with the divalent carbon atoms, D is determined predominantly by large one-center $n-\pi$ interactions on these carbons. In such a case, the quantity $(2S - 1)D$ measures the averaged $n-\pi$ interaction in the molecule. This will be derived in the following section. Since the term $(2S - 1)D$ for the nonet molecules occurs in the same range as that for the already known

(42) Brandon, R. W.; Closs, G. L.; Davoust, C. E.; Hutchison, C. A., Jr.; Kohler, B. E.; Silbey, R. *J. Chem. Phys.* **1965**, *43*, 2006–2016.

(43) Pryce, M. H. L. *Proc. Phys. Soc., London, Sect. A* **1950**, *A63*, 25; Abragam, A.; Pryce, M. H. L. *Proc. R. Soc. London, Ser. A* **1951**, *A205*, 135.

(44) Stone, A. J. *Proc. R. Soc. London, Ser. A* **1963**, *A271*, 424.

(45) The book cited in ref 39, p 745.

high-spin hydrocarbons ($S \geq 2$), the fine-structure parameters offer yet another evidence for the generation of **1**. In addition, it is possible to reproduce the observed D and E values by a semiempirical calculation on the basis of a probable molecular structure of **1** as described in the following section. Thus, both the observed g value and the fine-structure parameters lead to the conclusion that hydrocarbon **1** is in the nonet state, which we have already shown to be the ground state.

Since all the isomers are in nonet ground states and since the D and E values do not differ greatly, the observed spectral changes may be ascribed to moderate conformational changes of **1**. The principal axes of isomers I–IV listed in Table I provide information on their molecular conformations and orientations in the crystal. The Z axes—associated with the long axis of **1** as will be demonstrated by a semiempirical calculation—are approximately parallel with one another: The Z axes of isomers I, II, and IV coincide within 2° , and the Z axis of III makes angles of 6° , 5° , and 6° , respectively, to those of I, II, and IV. The stability of the direction of the molecular long axis in the crystal is to be expected with such a large molecule as **1**. Isomer III, with the largest D and the smallest E , has rather different directions of the principal axes from those of the other three.

When the nonet molecule changes according to $I \rightarrow II \rightarrow IV$, the Z axis moves its direction by $\theta_{II,I} = 2^\circ$ and $\theta_{II,IV} = -2^\circ$, while the X and Y axes rotate by $\phi_{I,II} = 13^\circ$ and $\phi_{II,IV} = -12^\circ$, about the old Z axis. On the other hand, the changes $I \rightarrow III \rightarrow IV$ gave $\theta_{I,III} = 6^\circ$, $\theta_{III,IV} = -6^\circ$ and $\phi_{I,III} = 50^\circ$, $\phi_{III,IV} = -48^\circ$. Thus, the latter route via III is accompanied by considerable rotation of the principal X and Y axes, from the corresponding conformational change in the crystal. Interestingly, the final isomer IV has almost the same fine-structure tensor as that of I both in magnitude and direction; the X , Y , and Z axes coincide within 1° . This suggests that the molecule rests finally in the same conformation adopted immediately after photolysis. Since the nonet molecules are embedded in the host crystal with energetically optimum orientations, knowledge of the orientation of the principal axes of the fine-structure tensor relative to the crystal provides valuable information about the molecular structure, as described below.

B. Semiempirical Calculation of the Fine-Structure Tensor.

Since the spin-orbit interaction is negligibly small for the hydrocarbon studied here, the first-order dipole-dipole interaction between the electron spins is the origin of the fine structure tensor. The ij component of the fine-structure tensor for a high-spin molecule is given by the expression

$$D_{ij} = \langle \frac{2}{3} \rangle (3e^2\hbar^2/4m^2c^2) [2!(2S-2)!/(2S)!] \sum_{p,q} \langle p(1)q(2) - q(1)p(2) \rangle (r_{12}^{-2}\delta_{ij} - 3i_{12}j_{12})/r_{12}^5 \langle p(1)q(2) \rangle$$

$$i, j = X, Y, Z \quad (9)$$

where $p(i)$ and $q(i)$ are the molecular orbitals occupied by the i th electrons which are orthonormal with each other.⁵ For hydrocarbons with electronic structures similar to **1**, there are three types of spin-spin interaction, i.e., $\pi-\pi$, $n-n$, and $n-\pi$ interactions. Higuchi has pointed out that the spin-spin interaction in such hydrocarbons arises predominantly from the one-center $n-\pi$ interaction at the divalent carbon atoms.^{5,6} Assuming that only the one-center $n-\pi$ interaction contributes to the spin-spin interaction and that the n electron is localized on the divalent carbon atom

$$D_{ij} = (e^2\hbar^2/2m^2c^2) [S(2S-1)]^{-1} \sum_{k \text{ MO}} \langle n_k(1)\pi_k(2) - \pi_k(1)n_k(2) \rangle (r_{12}^{-2}\delta_{ij} - 3i_{12}j_{12})/r_{12}^5 \langle n_k(1)\pi_k(2) \rangle \quad (10)$$

where $n_k(i)$ and $\pi_k(i)$ are the n orbital and the amplitude of molecular orbital on the k th divalent carbon atom, respectively. If we replace $\pi_k(i)$ with the $2p$ atomic orbital of the k th divalent carbon atom $p_k(i)$, the quantity denoted by the bracket becomes $\rho_{k,MO} \langle n_k(1)p_k(2) - p_k(1)n_k(2) \rangle (r_{12}^{-2}\delta_{ij} - 3i_{12}j_{12})/r_{12}^5 \langle n_k(1)p_k(2) \rangle$, where $\rho_{k,MO}$ is the spin density on the k th divalent carbon atom due to the singly occupied molecular orbital $\pi_k(i)$. The latter bracket is the ij element of such a $n-\pi$ interaction tensor \mathbf{d} inherent

to the divalent carbon atom, and it has the same principal values but different orientations for individual divalent carbon atoms. Thus, eq 10 can be rewritten as

$$D_{ij} = (e^2\hbar^2/2m^2c^2) [S(2S-1)]^{-1} \sum_{\text{MO } k} \sum \rho_{k,MO} (\mathbf{U}_k \cdot \mathbf{d} \cdot \mathbf{U}_k^\dagger)_{ij} \quad (11)$$

where \mathbf{U}_k is a unitary matrix which transforms the local symmetry axes for the divalent carbon moiety to the principal X , Y , Z axes referred to the molecular frame.

From eq 11, we obtain the expression for $D = (3/2)D_{ZZ}$ as

$$[S(2S-1)/N]D = (3e^2\hbar^2/4m^2c^2) \sum_{\text{MO}} \langle \rho_{k,MO} (\mathbf{U}_k \cdot \mathbf{d} \cdot \mathbf{U}_k^\dagger)_{ZZ} \rangle_k \quad (12)$$

where $\langle \rangle_k$ means the average over k , and N is the number of the divalent carbon atoms in the molecule. For hydrocarbons with similar electronic structures to **1**, N equals S . Thus, the term $(2S-1)D$ described in the preceding section may be regarded as a measure of the one-center $n-\pi$ interaction averaged over the whole molecule. This value reflects the electronic structure of these high-spin molecules (Table II). The value of 0.4050 for the case $S=1$ is a special case for a single divalent carbon atom devoid of the averaging process, which normally leads to cancellation among the elements of the tensors arising from different divalent carbon atoms.

Although one may calculate in principle the fine structure tensor from eq 9 using, e.g., INDO or ab initio molecular orbitals, the number of parameters necessary for the molecular structure of **1** is so large that such a calculation is not practical at present. Thus, in order to obtain information about the molecular structure, we have carried out a semiempirical calculation based on simplifying assumptions. We use eq 11 which takes only the one-center $n-\pi$ interaction into account, and we substitute a normalized empirical value $\mathbf{d}_{DPM}/\rho_{DPM}$ for \mathbf{d} in eq 11, where \mathbf{d}_{DPM} is the fine-structure tensor observed with diphenylmethylene ($S=1$)⁴² and ρ_{DPM} is a calculated spin density on the divalent carbon atom of diphenylmethylene. The semiempirical formula finally obtained is

$$D_{ij} = [S(2S-1)]^{-1} \sum_k (\rho_k/\rho_{DPM}) (\mathbf{U}_k \cdot \mathbf{d}_{DPM} \cdot \mathbf{U}_k^\dagger)_{ij}$$

$$i, j = X, Y, Z \quad (13)$$

where $\rho_k = \sum_{\text{MO}} \rho_{k,MO}$ and the constants $(e^2\hbar^2/2m^2c^2)$ are lumped together into \mathbf{d}_{DPM} . It is possible to use the experimental value directly determined from the hyperfine coupling of $^{13}\text{C}^{42}$ or from proton ENDOR⁴⁶ instead of the calculated ρ_{DPM} . However, we used the calculated values for both ρ_k and ρ_{DPM} : they are more appropriate in the sense that they are of the same nature and of the same degree of approximation.

C. Probable Molecular Conformations of the Nonet Hydrocarbons. Using eq 13, we have determined probable molecular conformations for isomers I–IV not only most appropriate to interpret the observed D and E and their principal axes but also consistent with the structure of the benzophenone host crystal. For calculating the fine-structure tensor, the following simplifying assumptions were made:

(1) Equal bond angles α are assumed at each divalent carbon atom. Higuchi has reported a theoretically probable bond angle of 144 – 150° for triplet diphenylmethylene⁴⁷ and near 140° for quintet m -phenylenebis(phenylmethylene),⁹ while Hutchison et al. have observed angles of 154° ⁴² and 148° ⁴⁶ for diphenylmethylene. We have varied α from 140° to 150° .

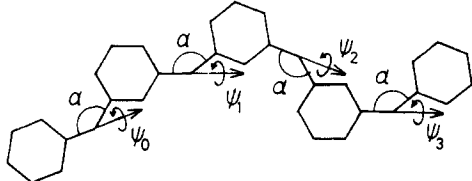
(2) The molecule is first assumed to be planar except for the twist of the two outermost phenyl groups. The restriction is relaxed afterward.

(3) By simple LCAO-MO theory, the spin densities are $\rho_{DPM} = 0.4000$, while they are $\rho_1 = 0.4041$ for the outer divalent carbon atom and $\rho_2 = 0.4082$ for the inner two divalent carbon atoms.

(4) For \mathbf{d}_{DPM} , the following observed values⁴² are used: $d_{DPM,xx} = -0.15420$, $d_{DPM,yy} = -0.11584$, $d_{DPM,zz} = 0.27003 \text{ cm}^{-1}$, where

(46) Hutchison, C. A., Jr.; Kohler, B. E. *J. Chem. Phys.* **1969**, *51*, 3327.

(47) Higuchi, *J. Bull. Chem. Soc. Jpn.* **1971**, *44*, 2634–2638.

Table III. Calculated D , E , and E/D Values and the Rotation Angles for the Most Probable Conformations of the Nonet Isomers I-IV^a


isomer	D , cm^{-1}	E , cm^{-1}	E/D	ψ_0	ψ_1	ψ_2	ψ_3	ϕ
I, IV	0.04061	-0.00883	-0.217	0°	0°	0°	0°	
II	0.04065	-0.00794	-0.195	0°	+30°	-30°	+30°	12°
III	0.03613	-0.00399	-0.110	0°	+30°	+30°	+30°	32°

^a For all the isomers, the best bond angle α is 140°. ϕ is the rotation angle of the X and Y axes in the conformational changes.

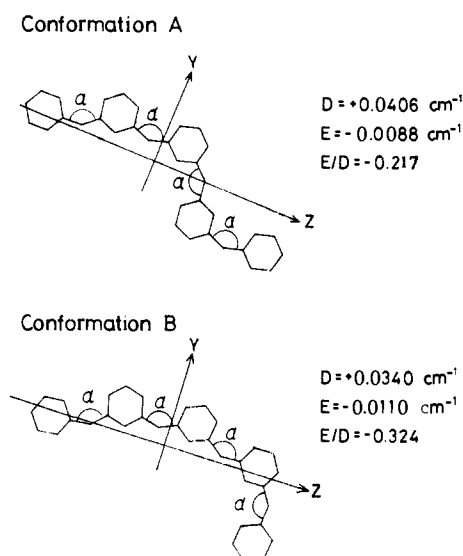


Figure 9. Probable molecular conformations of the isomer I. The fine-structure parameters D and E and the principal axes are those calculated for $\alpha = 140^\circ$. The most probable molecular conformation A and a less probable conformation B (see text) are shown.

x is perpendicular to the molecular plane and y is along the bisector of the bond angle of the divalent carbon atom.

On choosing a most probable conformation, we have looked for the consistency with the crystal structure as well as taken into account the E/D ratio rather than the absolute values of D and E . The E/D ratio is a more reliable index for the molecular structure of this type of hydrocarbons, as pointed out theoretically by Higuchi,⁵ since factors due to incomplete approximations in estimation of molecular integrals cancel each other.

Hydrocarbon **1** can take 36 different conformations even when only planar structures are assumed. The probable conformations for isomer I under the restriction of planarity and the calculated D and E values are shown in Figure 9; isomer IV is substantially the same as I. For the bond angle α varied, the best value is found to be 140° . The Z axis is nearly along the molecular long axis and the X axis is perpendicular to the molecular plane. Conformation A is the most probable for isomers I and IV: it gives a positive sign for D and its E/D ratio comes closest to the observed value of -0.125 for the possible conformations which can be placed without difficulty in the three-dimensional host crystal structure. In view of the approximation in deriving eq 13 and of the simplifying assumptions, the results obtained here are rather satisfactory. This methodology may be useful for dealing with large high-spin molecules such as **1**.

The projection of conformation A onto the ab plane of the host crystal is shown in Figure 10. This orientation requires three substitutional sites of benzophenone over the two unit cells. The 3:1 ratio is the minimum demanded by substitution of **1** with its molecular size. Figure 9 also shows another probable conformation B. This conformation is less probable judging from the deviation in the E/D ratio and from the more severe requirement of four

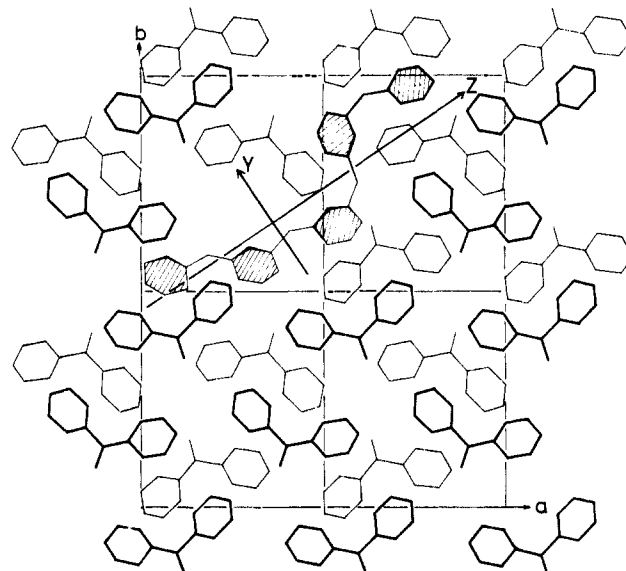


Figure 10. Crystal structure of benzophenone and the orientation of the isomer I in the crystal. The molecules drawn with thin lines have their mid points at $z = 0$ and those with heavy lines at $z = 1/2$, where z is the height along the c axis.

substitutional sites over the two unit cells. However, its calculated D value is even closer to the observed, and it seems difficult to rule out completely the possibility of the B conformation.

Probable conformations of isomers II and III are to be derived from conformation A because II and III are produced from I. Table I shows that II is different from I in their D and E values but their axes are close to each other, whereas III is different from I both in their D and E values and in their axes. The E/D ratios of II and III are -0.070 and -0.065 , to be compared with -0.125 of I and IV. These small values together with the considerable rotation of the X and Y axes of III mentioned before could not be reconciled with planar structures. Therefore, we removed the restriction of planarity and we took into account the twist of the phenyl groups. Under the constraint of the present semiempirical calculation, this twist may be dealt with as a rotation of the $n-\pi$ interaction tensor \mathbf{d} on each divalent carbon atom. In the calculation, each phenyl ring was independently twisted by ψ_i ($i = 1, 2, \text{ and } 3$) about the bond between the divalent carbon and the ring carbon in the range of -30° to $+30^\circ$ starting from conformation A. Outside of this range, the molecular structure became too bulky for incorporation within the host crystal lattice, and moreover the π spin densities based on the simple LCAO-MO calculation seriously lost their meaning.

The results of the calculation are summarized in Table III. Although they failed to agree quantitatively with the observed values, the trend of decreasing E/D and E values with the change from I to II and to III is reproduced by increasing the twist angles ψ_i . Rotations about each bond all in the same direction (internal *in-phase* rotation) left the Z axis almost unchanged, while they changed the X and Y axes greatly around the Z axis. On the other hand, using alternate signs of ψ_i along the molecular chain (internal

out-of-phase rotation) led to only small changes for each principal axis. The best ψ_i 's obtained for II and III are given in Table III. The angle ψ_0 was taken as zero in this calculation, because the principal axes of the \mathbf{d} tensor on the first divalent carbon atom were chosen as the reference coordinate system. The last column gives the rotation angle ϕ of the X and Y axes in the conformational changes calculated from these ψ_i 's: the angles 12° for II and 32° for III are in qualitative agreement with the observed values of 13° and 50° , respectively. Thus, the conformational changes I \rightarrow II \rightarrow IV and I \rightarrow III \rightarrow IV are most probably ascribable to the out-of-phase and in-phase rotations of the phenyl groups, respectively. Further improvement of the numerical values seems beyond the scope of our semiempirical calculation. Investigation of the structure in more detail requires direct structural data such as those provided by electron-nuclear double resonance (ENDOR) as well as more advanced calculations including two-center interactions and structural optimization.

Since the above model consistently interprets the trend of the E/D value and the change in the direction of the principal axes, it may be concluded that the twist of the phenyl groups is responsible for the marked spectral changes at 64 and 92 K. In previous papers, a similar phenomenon was reported for biphenyl-3,3'-bis(phenylmethylene) which has low-lying singlet, triplet, and quintet states.^{11,40} For this molecule, the conformational change took place at 145 K in single crystals of benzophenone, and two isomers arising from the twist about the central C-C bond of the biphenyl skeleton were observed.

Conclusion

We have investigated by single-crystal ESR a novel hydrocarbon, *m*-phenylenebis[(diphenylmethylene-3-yl)methylene] (**1**). The results can be summarized as follows: (1) A calculation based on the spin Hamiltonian (eq 1) with $S = 4$ showed excellent agreement with the observed resonance fields and intensities as well as their angular dependence in the *ab*, *bc*, and *ca* planes of a benzophenone crystal. (2) The temperature dependence of the total signal intensity demonstrated that the observed nonet state is the lowest level, below the levels with $S = 0, 1, 2$, and 3. Static magnetic susceptibility measurements support this conclusion.¹⁶ (3) The isotropic g value close to the free spin value is consistent with **1** being composed only of carbon and hydrogen atoms with very small spin-orbit coupling constants. The same conclusion stems from the absence of the fine-structure terms higher than quadratic in S . (4) As shown in Table II, the observed D and E values are consistent with those of the known high-spin hydrocarbons with similar electronic structures. In particular, rather constant $(2S-1)D$ values are observed. They measure the averaged $n-\pi$ interaction in these hydrocarbons. (5) On the basis of a probable molecular structure for **1**, the semiempirical formula (eq 13) derived in this paper explains well the observed D and E values as well as the direction of the principal axes. All the evidence strongly supports formation of the nonet hydrocarbon **1** in benzophenone crystals upon photochemical decomposition of the *m*-phenylenebis[*m*-(α -diazobenzyl)phenyldiazomethane] precursor.

In addition, marked irreversible spectral changes (Figure 6) occur at 64 and 92 K on warming the sample from 4.2 K. They come from the twist of the phenyl rings, as accounted for in our semiempirical calculation. The most probable conformations of the four isomers thus detected were obtained. All four isomers were nonet in the ground state. This means that the mechanism for parallel alignment of the spins in the molecule is stable to conformational changes. These experimental findings obey the prediction by Longuet-Higgins that the number of singly occupied NBMO's is invariant to the individual resonance integrals.¹⁸ This stability to conformational change should be helpful in designing high-spin molecules. The photochemical reaction generating **1** is also interesting in itself, a one-photon photodissociation process in benzophenone host crystals is suggested by ESR.

The novel hydrocarbon has the highest spin multiplicity found among organic as well as inorganic molecules. Consideration of

the series of high-spin hydrocarbons in Table II strongly supports the notion that an organic system with a very large number of parallel spins might be obtained with proper design of its molecular structure on the basis of its topological symmetry. Extension of the high-spin hydrocarbon reported here may be one of the most promising approaches to organic ferromagnets.

Acknowledgment. Professor Pierre Laszlo of the University of Liège deserves special thanks for a careful reading and refinement of the manuscript. This work was supported by the Joint Studies Program (1983-1985) of the Institute for Molecular Science.

Appendix

Resonance Fields and Relative Transition Probabilities. The following notations are used in the subsequent equations.

$$H_0 = h\nu/g\beta$$

$$D_0 = -D_{zz}$$

$$D_1 = D_{zx} + iD_{zy}$$

$$D_2 = D_{xx} - D_{yy} + 2iD_{xy}$$

$$B_1 = (D_{xx} - D_{yy})/2g\beta$$

$$D'_i = D_i/g\beta$$

where β is the Bohr magneton, $g^2 = \mathbf{h}\cdot\mathbf{g}\cdot\mathbf{g}\cdot\mathbf{h}$, and \mathbf{h} is the unit vector along the external magnetic field. Here $h\nu$ is the microwave energy and x , y , and z are the laboratory coordinates, the z axis being taken along the static magnetic field. In the following, $\text{Re}\{Z\}$ means the real part of Z . Only the allowed transitions $\Delta M_S = \pm 1$ are given.

The resonance fields to third order:

$$H_{\pm 4 \leftrightarrow \pm 3} = H_0 \pm (21/2)D_0' - [(217/2)|D_1|^2 - (35/8) \times |D_2|^2]/[H_0 \pm (21/2)D_0'] \mp [D_0'\{(5607/4)|D_1|^2 - (63/4)|D_2|^2\} + (1995/4) \text{Re}\{D_1'^2 D_2'^*\}]/H_0^2 \quad (\text{A1})$$

$$H_{\pm 3 \leftrightarrow \pm 2} = H_0 \pm (15/2)D_0' - [(73/2)|D_1|^2 + (1/8)|D_2|^2]/[H_0 \pm (15/2)D_0'] \mp [D_0'\{(405/4)|D_1|^2 + 45|D_2|^2\} - (375/4) \text{Re}\{D_1'^2 D_2'^*\}]/H_0^2 \quad (\text{A2})$$

$$H_{\pm 2 \leftrightarrow \pm 1} = H_0 \pm (9/2)D_0' - [(-23/2)|D_1|^2 + (25/8) \times |D_2|^2]/[H_0 \pm (9/2)D_0'] \pm [D_0'\{(1197/4)|D_1|^2 - (99/2)|D_2|^2\} + (945/4) \text{Re}\{D_1'^2 D_2'^*\}]/H_0^2 \quad (\text{A3})$$

$$H_{\pm 1 \leftrightarrow 0} = H_0 \pm (3/2)D_0' - [(-71/2)|D_1|^2 + (37/8) \times |D_2|^2]/[H_0 \pm (3/2)D_0'] \pm [D_0'\{(639/4)|D_1|^2 - (81/4)|D_2|^2\} + (435/4) \text{Re}\{D_1'^2 D_2'^*\}]/H_0^2 \quad (\text{A4})$$

The relative transition probabilities to second order:

$$I_{\pm 4 \leftrightarrow \pm 3} = 2[1 \pm 7B_1/[H_0 \pm (21/2)D_0'] + \{(-77/2)|D_1|^2 + (21/4)|D_2|^2 - (147/2) \text{Re}\{D_1'^2\} + (63/2)D_0' \text{Re}\{D_2'\}\}/H_0^2] \quad (\text{A5})$$

$$I_{\pm 3 \leftrightarrow \pm 2} = (7/2)[1 \pm 5B_1/[H_0 \pm (15/2)D_0'] + \{(-77/2) \times |D_1|^2 + (3/2)|D_2|^2 - (75/2) \text{Re}\{D_1'^2\} + 9D_0' \text{Re}\{D_2'\}\}/H_0^2] \quad (\text{A6})$$

$$I_{\pm 2 \leftrightarrow \pm 1} = (9/2)[1 \pm 3B_1/[H_0 \pm (9/2)D_0'] + \{(-77/2) \times |D_1|^2 - |D_2|^2 - (27/2) \text{Re}\{D_1'^2\} - 6D_0' \text{Re}\{D_2'\}\}/H_0^2] \quad (\text{A7})$$

$$I_{\pm 1 \leftrightarrow 0} = 5[1 \pm B_1/[H_0 \pm (3/2)D_0'] + \{(-77/2)|D_1|^2 - (9/4)|D_2|^2 - (3/2) \text{Re}\{D_1'^2\} - (27/2)D_0' \text{Re}\{D_2'\}\}/H_0^2] \quad (\text{A8})$$

Registry No. 1, 85566-03-6; **2**, 85566-04-7; *m*-BrC₆H₄Me, 591-17-3; *m*-CNC₆H₄CN, 626-17-5; Me(*m*-C₆H₄CO)₂-*m*-C₆H₄Me, 85566-05-8; Me(*m*-C₆H₄CO)₂-*m*-C₆H₄CO₂H, 85566-06-9; CO₂H(*m*-C₆H₄CO)₂-*m*-C₆H₄CO₂H, 85566-07-0; ClCO(*m*-C₆H₄CO)₂-*m*-C₆H₄COCl, 85566-08-1; Ph(CO-*m*-C₆H₄)₄H, 85566-09-2; 3,3'-dibenzoylisophthalophenone tetrahydrazone, 85566-10-5.